Supplementary Information

Efficient Photocatalytic CO$_2$ Reduction Coupled with Selective Styrene Oxidation over Modified g-C$_3$N$_4$/BiOBr Composite with High Atom Economy

Peng Bai,[a,b] Yicheng Zhao,[a,b]* Yongdan Li[c]

[a]State Key Laboratory of Chemical Engineering (Tianjin University), Tianjin Key Laboratory of Applied Catalysis

Science and Technology, School of Chemical Engineering and Technology, Tianjin University, Tianjin, 300072, China

[b]Collaborative Innovation Center of Chemical Science and Engineering (Tianjin), Tianjin, 300072, China

[c]Department of Chemical and Metallurgical Engineering, Aalto University, Kemistintie 1, FI-00076 Aalto, Finland
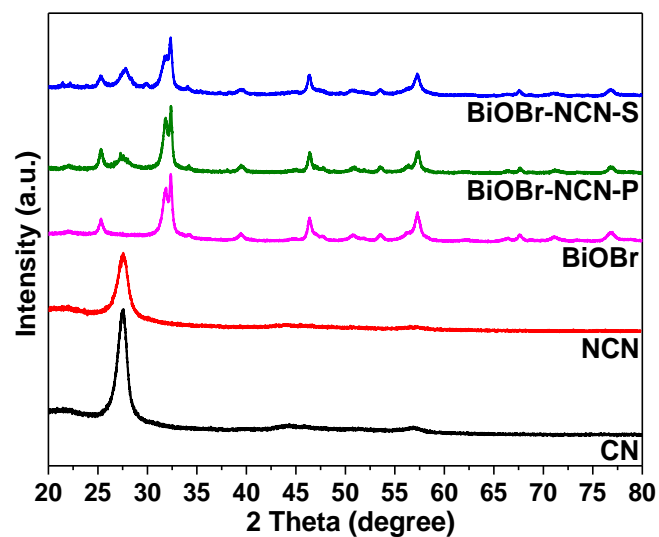
*Email: zhaoyicheng@tju.edu.cn

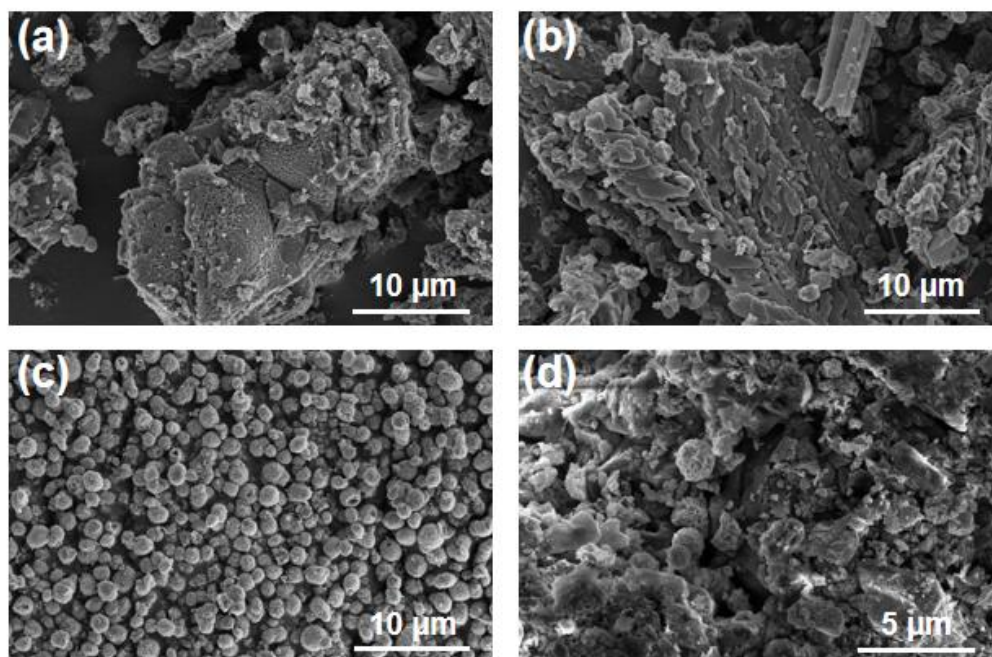**Fig. S1** XRD patterns of the samples.

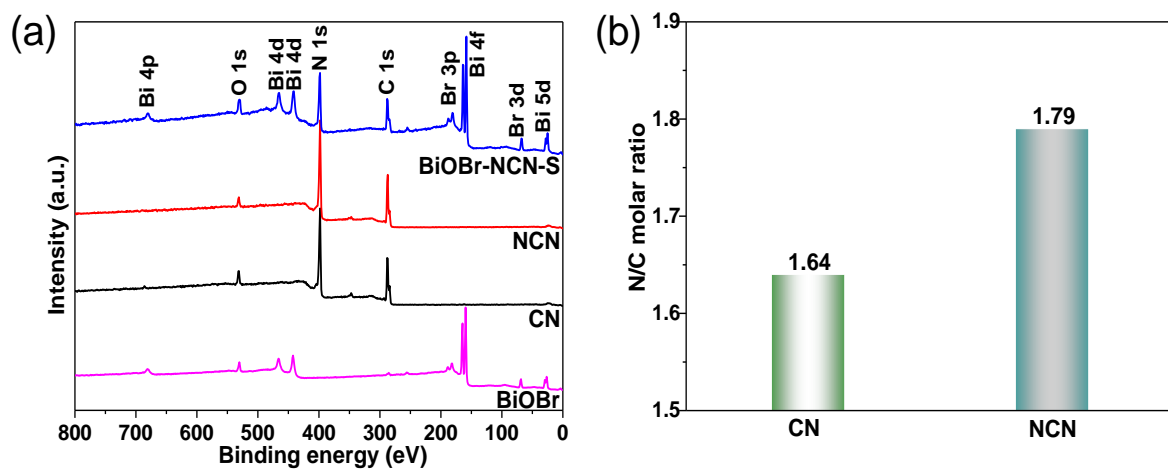**Fig. S2** SEM images of (a) CN, (b) NCN, (c) BiOBr and (d) BiOBr-NCN-S.

Fig. S3 (a) XPS survey spectra of the samples. (b) N/C molar ratio on the surface of CN and NCN based on the XPS results.
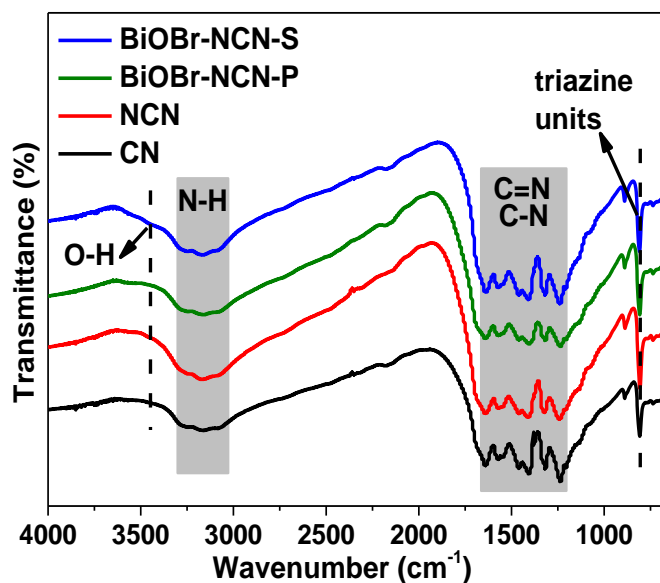
Fig. S4 FTIR spectra of the samples.

The strong sharp peak at 810 cm^{-1} corresponds to the vibration of triazine units of CN. The pronounced absorption in 1230-1640 cm^{-1} is attributed to the stretching vibration of CN heterocycles including sp^2 C=N stretching vibrations and out-of-plane bending modes of sp^3 C-N bonds. The broad band in 3050-3300 cm^{-1} is related to residual N-H components. Compared with CN, a stronger band at 3050-3300 cm^{-1} of NCN indicates more uncondensed amino groups, demonstrating that the carbocyclic structure of CN is partially destroyed after the modification with NH$_4$Cl. Moreover, a new weak absorption peak at about 3450 cm^{-1} is found in the result of BiOBr-NCN-S, which is ascribed to the O-H bond of hydroxyl groups adsorbed on the oxygen vacancies, indicating that more oxygen vacancies are formed on the surface of BiOBr-NCN-S.
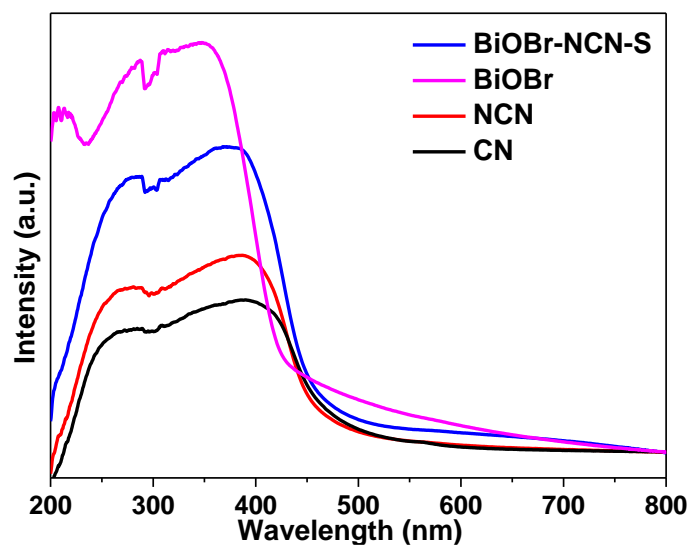
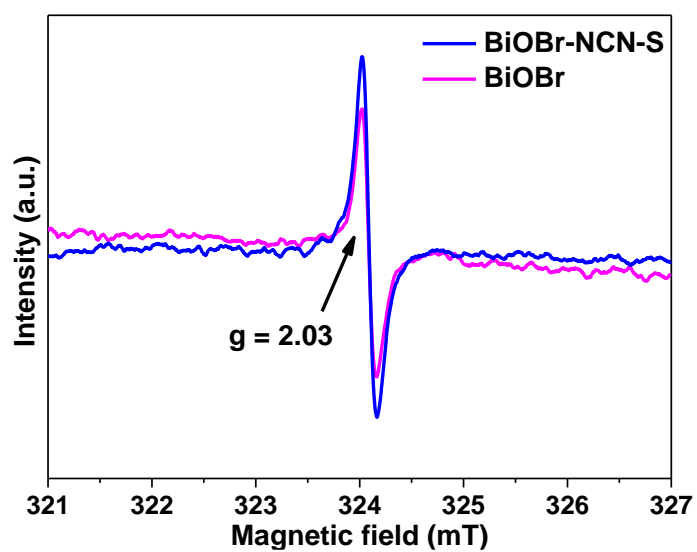**Fig. S5** UV-vis absorption spectra of the samples.

Fig. S6 EPR spectra for the detection of oxygen defects in BiOBr and BiOBr-NCN-S.

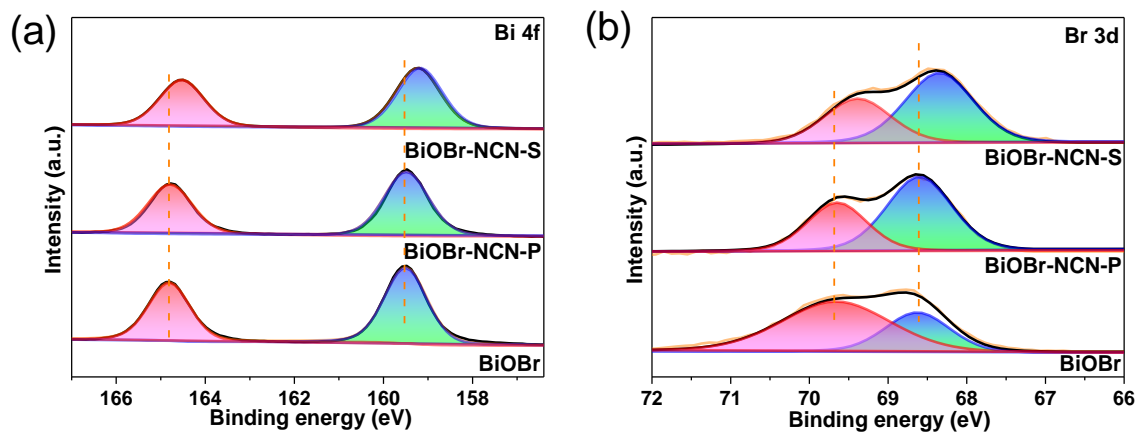The characteristic peaks at g = 2.03 are assigned to the oxygen defects.

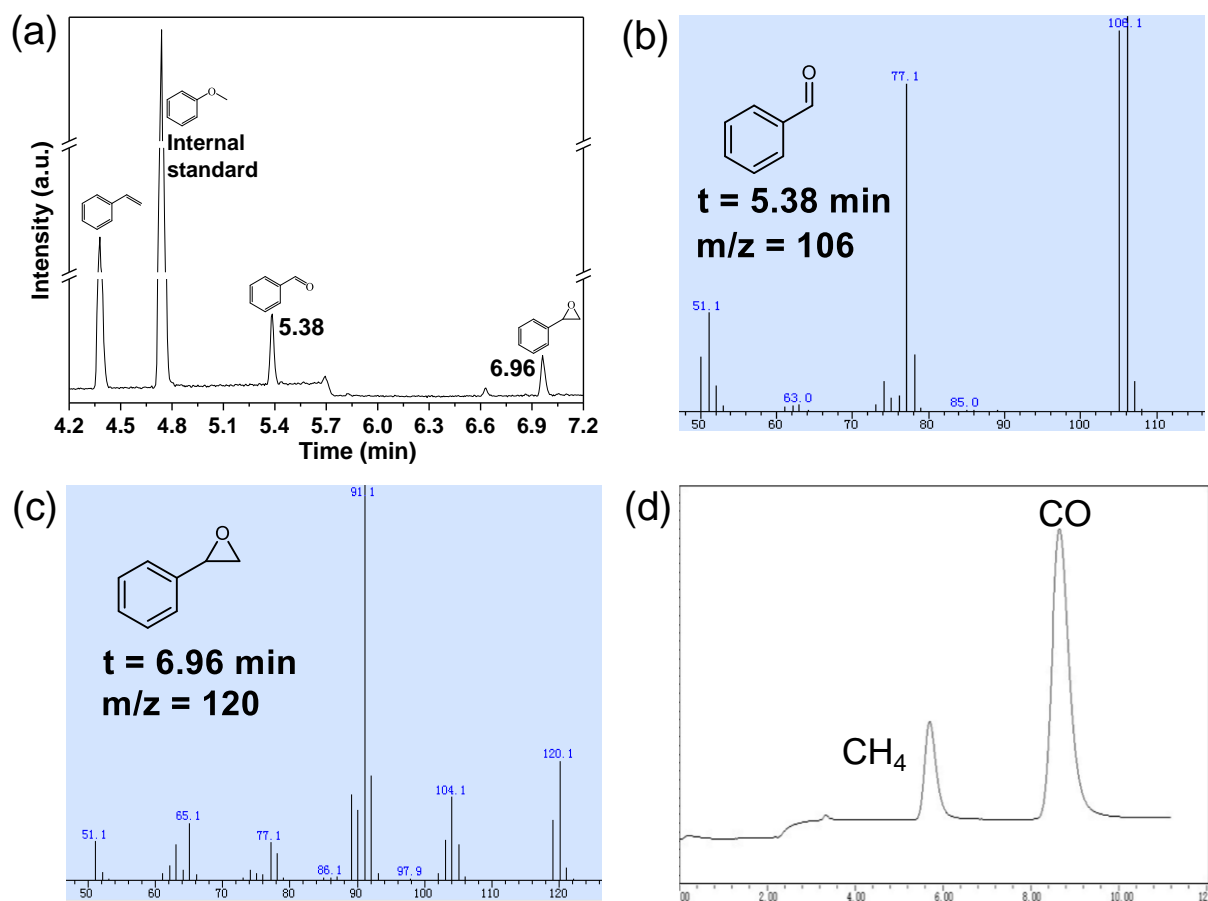**Fig. S7** High-resolution XPS spectra of (a) Bi 4f and (b) Br 3d of various photocatalysts.

Fig. S8 (a) GC analysis results of styrene oxidation products. Only benzaldehyde (BD) and styrene oxide (SO) products are generated in the liquid phase. (b, c) GC-MS analysis results of BD and SO products. (d) GC analysis results of CO_2 reduction products.
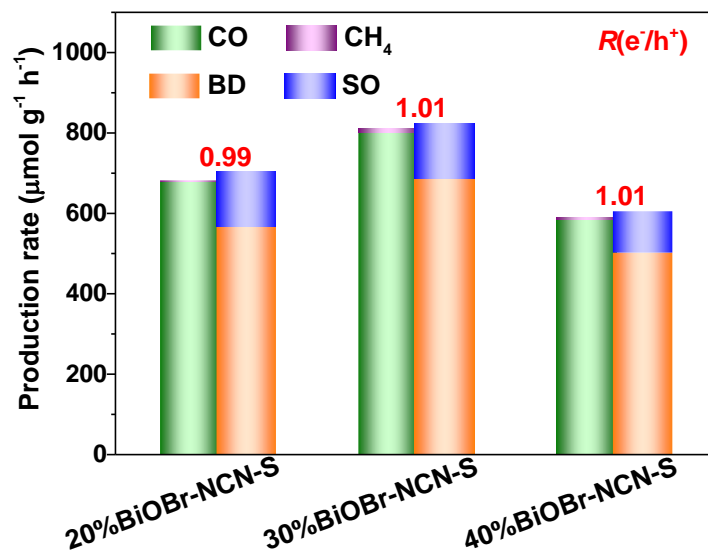
Fig. S9 Photocatalytic redox performance of the catalysts with various BiOBr contents.
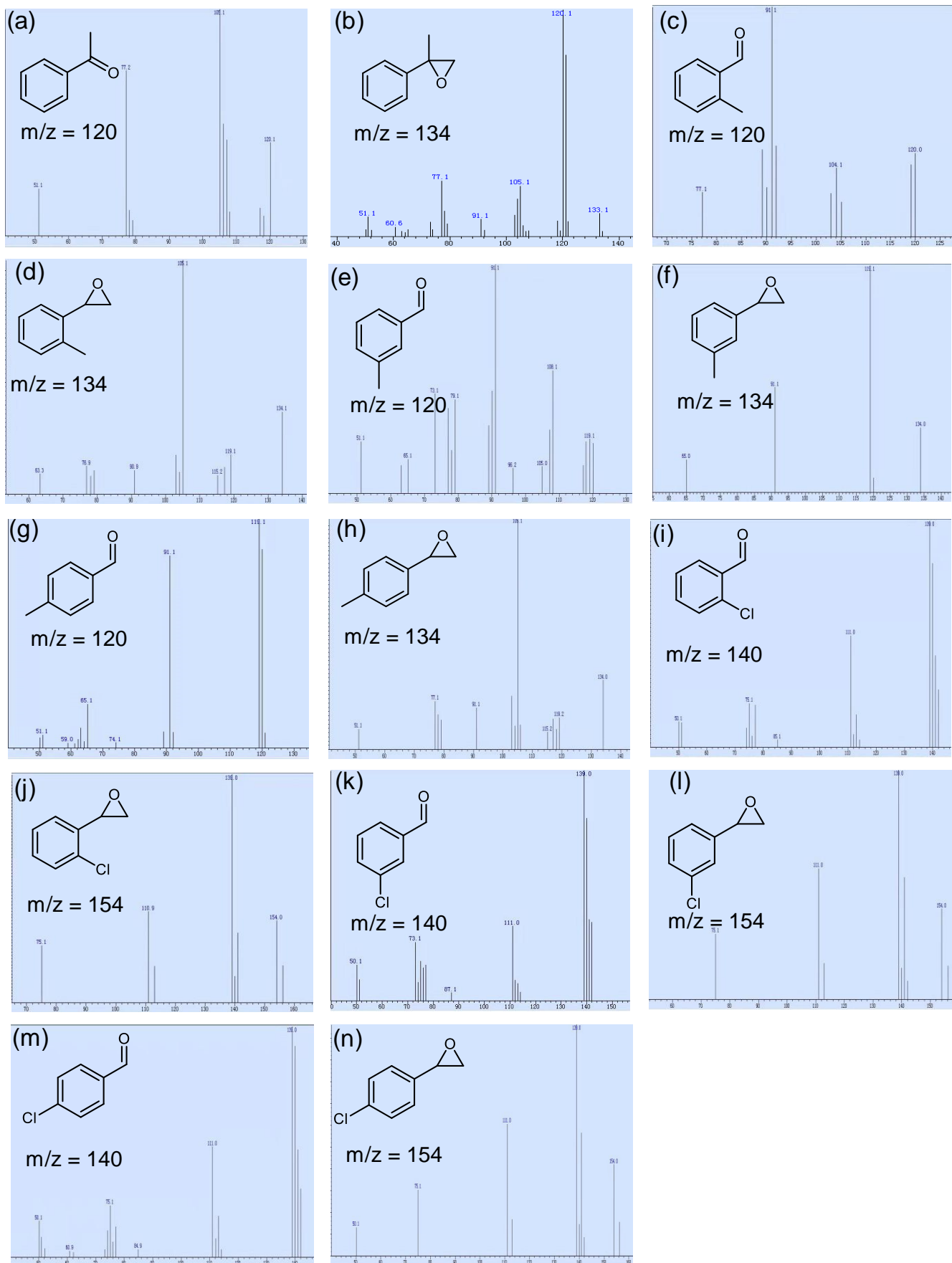
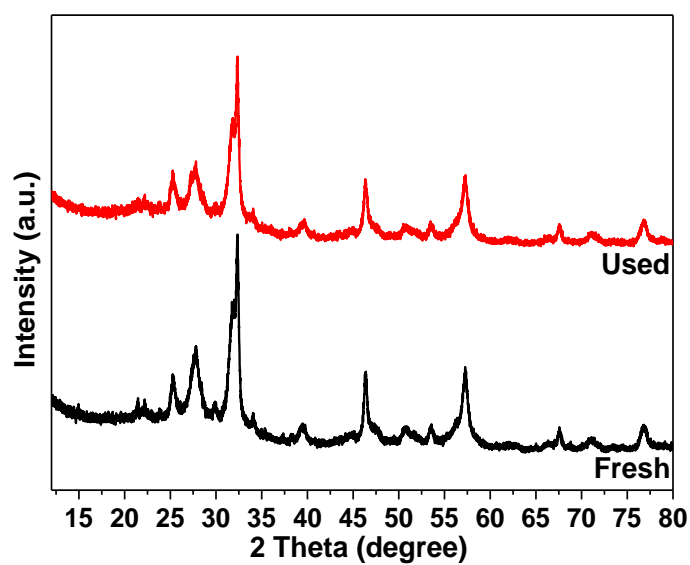**Fig. S10** GC-MS analysis results of oxidation products.

Fig. S11 XRD patterns of the BiOBr-NCN-S sample before and after reaction.
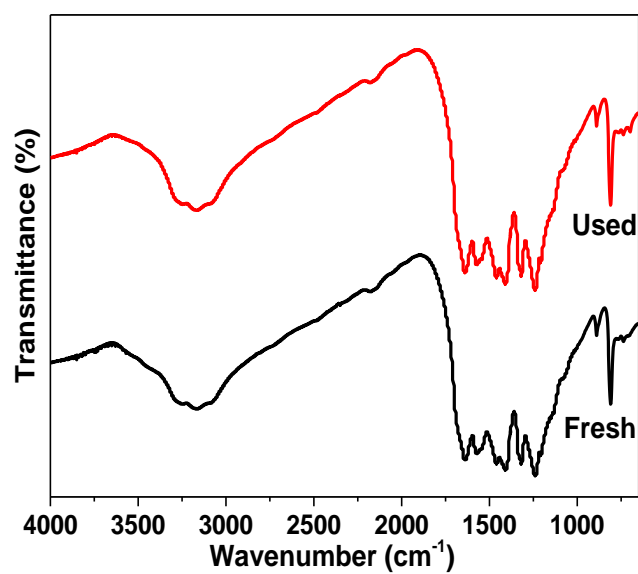

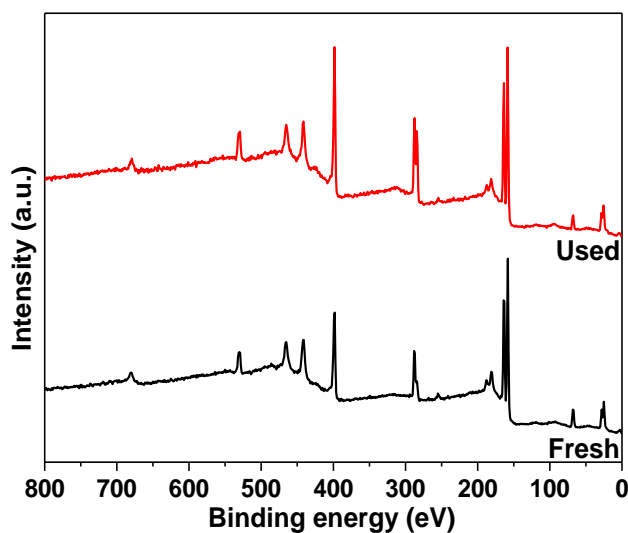**Fig. S12** FTIR spectra of the BiOBr-NCN-S sample before and after reaction.

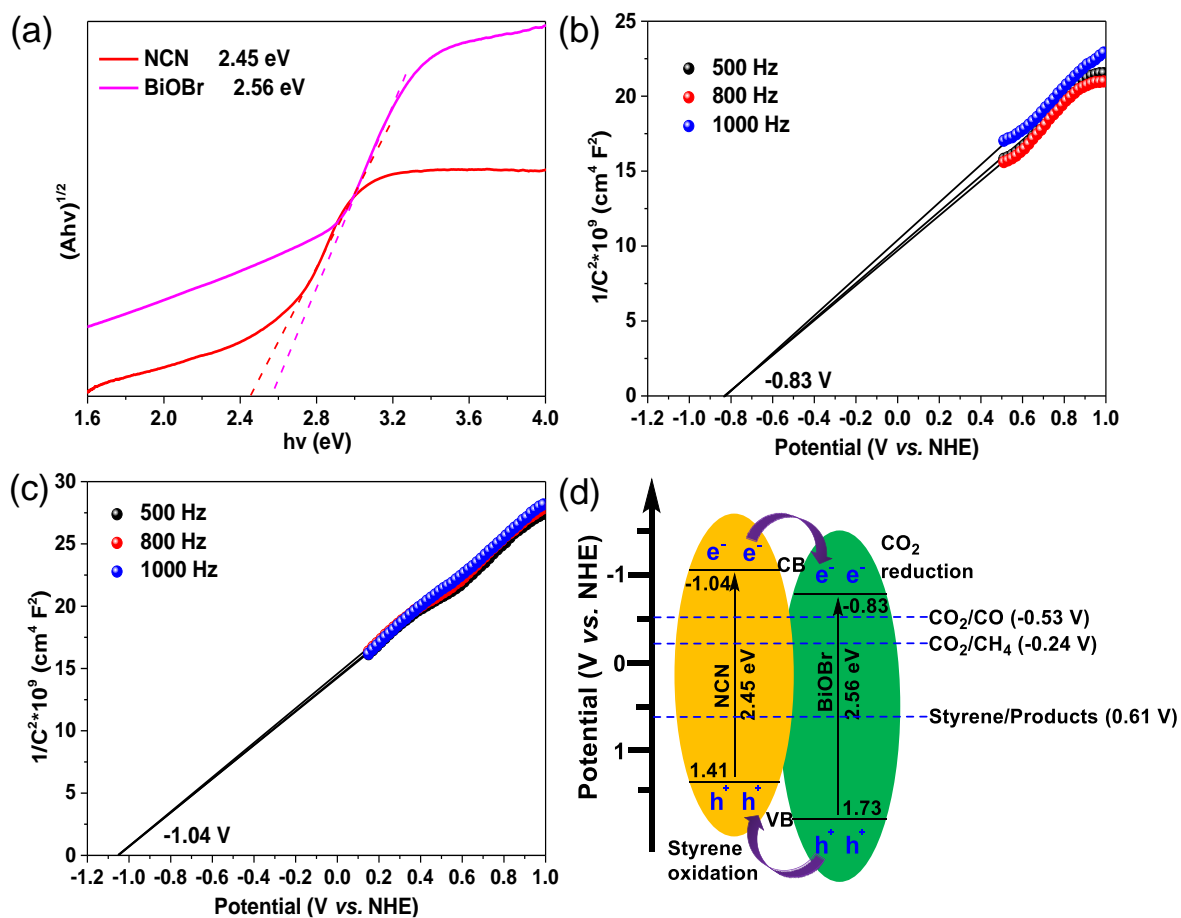**Fig. S13** XPS survey spectra of the BiOBr-NCN-S sample before and after reaction.

Fig. S14 (a) The plots of $(Ah\nu)^{1/2}$ versus photon energy for NCN and BiOBr. Mott-schottky plots of (b) BiOBr and (c) NCN under different frequencies. (d) Schematic band structure evolution of BiOBr-NCN-S composite.
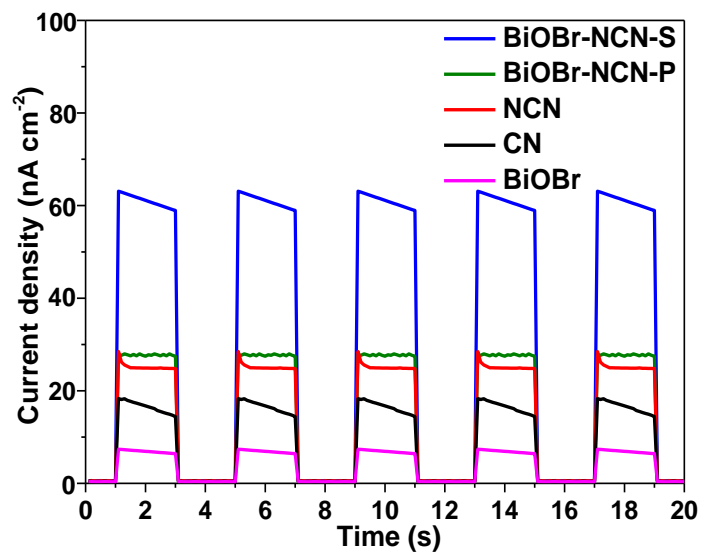
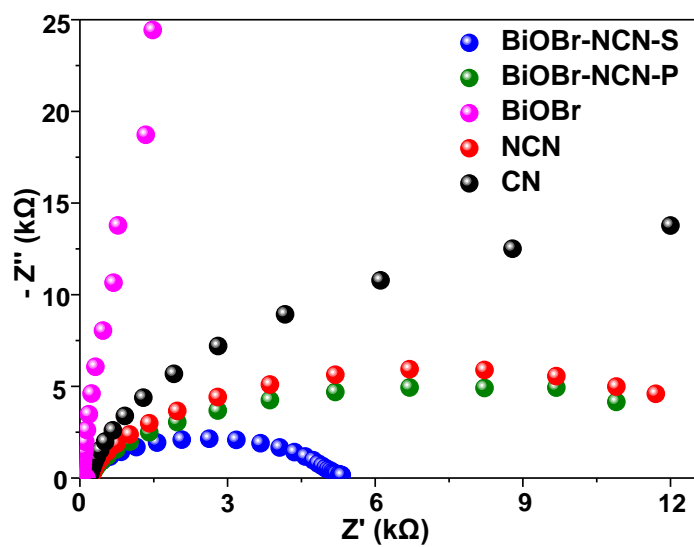**Fig. S15** Photocurrent responses of different samples.

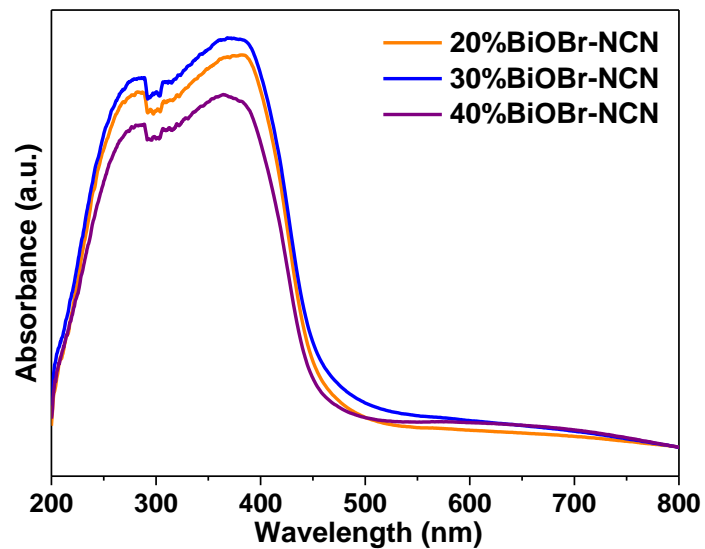**Fig. S16** EIS curves of different samples.

Fig. S17 UV-vis absorption of the catalysts with various BiOBr contents.
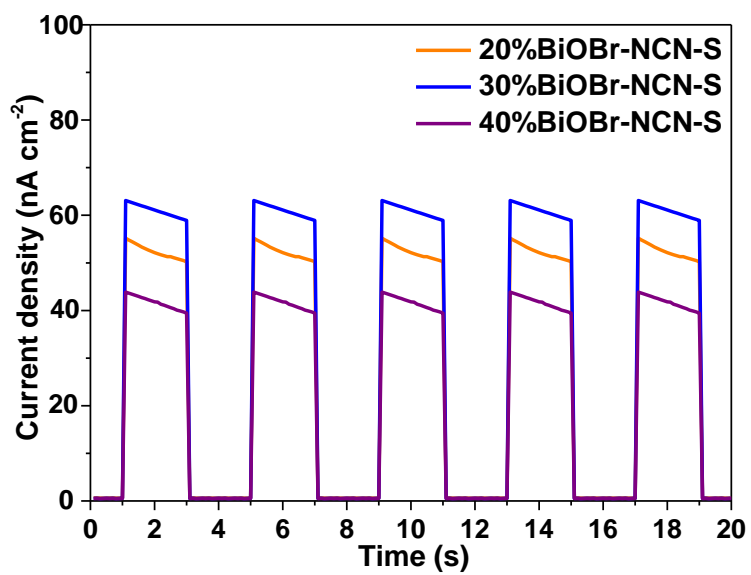

Fig. S18 Photocurrent responses of the catalysts with various BiOBr contents.
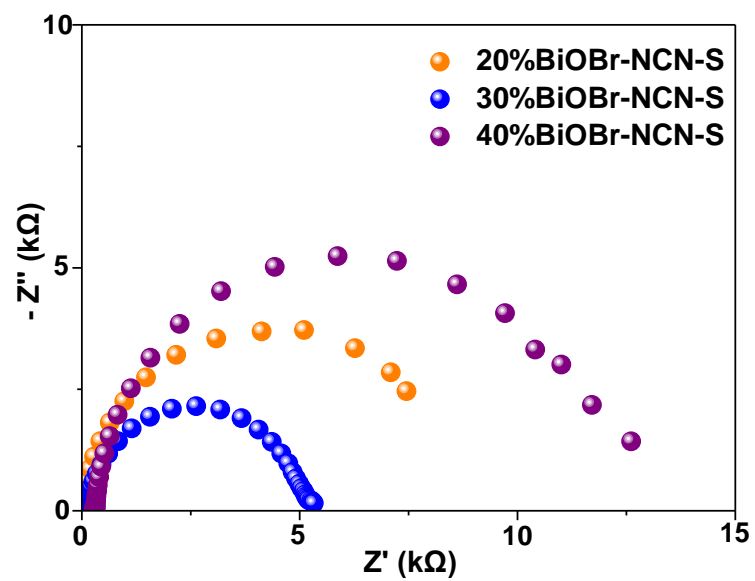
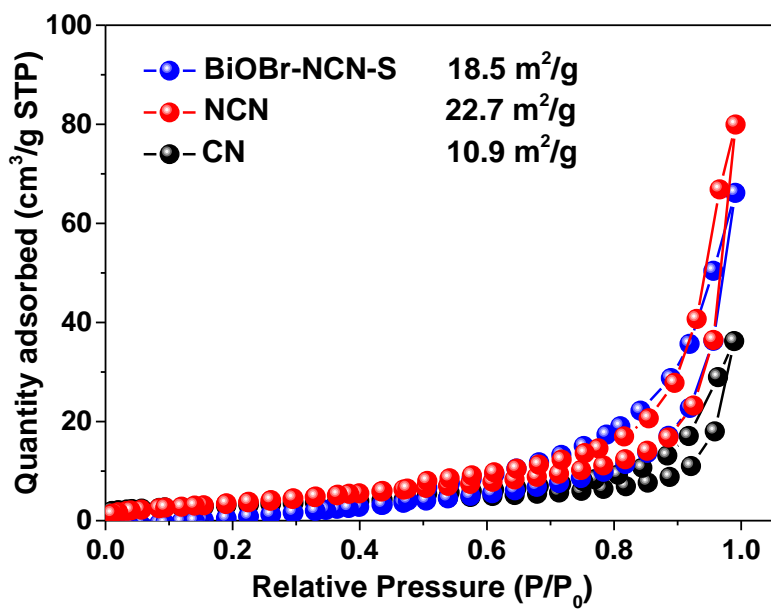**Fig. S19** EIS curves of the catalysts with various BiOBr contents.

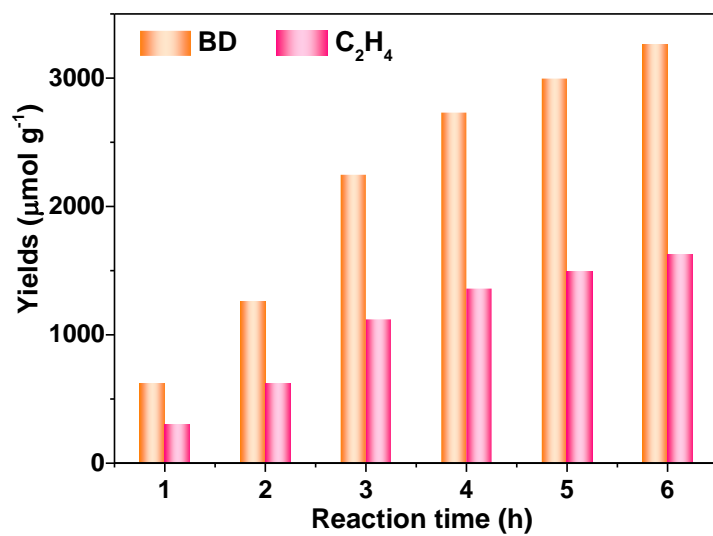**Fig. S20** N$_2$ adsorption isotherms of CN, NCN and BiOBr-NCN-S.

Fig. S21 Time-yield plots of the BD and C_2H_4 over BiOBr-NCN-S.
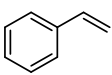
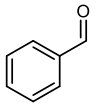**Table S1.** The results of elemental analysis.
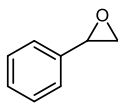
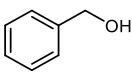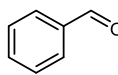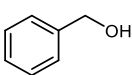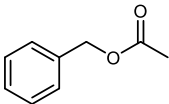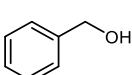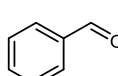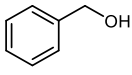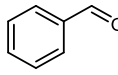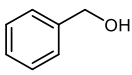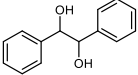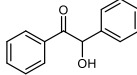| Sample	Atomic content (%)			Atomic ratio of N/C
	N	**C**	**H**	
CN	49.5	32.5	18.0	1.52
NCN	48.8	32.3	18.9	1.51

Table S2. Representative summary of photocatalytic CO_2 reduction to CO.
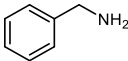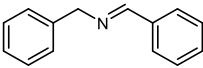
Catalyst	photosensitizer	Sacrificial agent	Reducing reagent	CO yield (μmol g^{-1} h^{-1})	CO selectivity	AQE	Ref.
BiOBr-NCN-S	None	None	SE	802	96.2%	1.26%	This work
BiOBr-NCN-S	None	None	H_2O	59	90.2%	0.21%	This work
Cu-SAEB[a]	None	None	H_2O	236	＞99.0%	1.49%	1
$Cu_2S@R_{OH}$-$NiCo_2O_3$ DSNBs[b]	[Ru(bpy)$_3$]Cl$_2$	TEOA	H_2O	7067	72.0%	1.01%	2
MAF-34-CoRu[c]	None	None	H_2O	11	100.0%	0.015%	3
Cu/CN-0.25	None	None	H_2O	11	59.3%	1.32%	4
3DOM CdSQD/NC[d]	bipyridine/CoCl$_2$	None	BA[f]	5210	89.6%	2.9%	5
Pt/C/CdS@ZnIn$_2$S$_4$/CoO$_x$	None	None	H_2O	329	88.6%	0.34%	6
In@Mo$_2$C-d[e]	None	TEA	H_2O	234	97.3%	7.2%	7
Co-Bi$_3$O$_4$Br-1	None	None	H_2O	107.1	99.4%	0.91%	8

[a] Cu-SAEB: N-Cu$_1$-S single-atom electron bridge. [b] Cu$_2$S@R_{OH}-NiCo$_2$O$_3$ DSNBs: double-shelled nanoboxes, with an outer shell of hydroxy-rich nickel cobaltite nanosheets and an inner shell of Cu$_2$S. [c] MAF-34-CoRu: [Co$_3$Ru$_4$(ip)$_{12}$]Cl$_2$. [d] 3DOM CdSQD/NC: 3D ordered macroporous N-doped carbon (NC) supported CdS quantum dots. [e] d: annealed in H$_2$/Ar (5%) at 600 °C for 3 h. [f] Benzylamine. CO selectivity (%) = 2n(CO)/[2n(CO) + 8n(CH$_4$) + 2n(H$_2$)].

Table S3. Representative summary of photocatalytic CO_2 reduction coupled with organic selective oxidation.

Catalyst	Solvent	Substrate	Oxidation product(s) (Yield(s) / μmol g⁻¹ h⁻¹)		Reduction product(s) (Yield(s) / μmol g⁻¹ h⁻¹)		Ref.
BiOBr-NCN-S	Acetonitrile	styrene	benzaldehyde (684)	styrene oxide (139)	CO (802)	CH_4 (8)	This work
g-CN/POM/[Re][a]	Acetonitrile	cyclohexene	benzene (12)	cyclohexadiene (11)	CO (21)		9
Ag-TiO₂	Acetonitrile	benzyl alcohol	benzaldehyde (33)		CH_3OH (9)		10
Cu₂O/Cu	Acetonitrile	benzyl alcohol	benzyl acetate (117)		CO (0.7)	HCOOH (3)	11
Cu₂O-RGO/BiVO₄[b]	Acetonitrile	benzyl alcohol	benzaldehyde (9)		HCOOH (3)		12
FAPbBr₃/Bi₂WO₆[c]	Trifluorotoluene	benzyl alcohol	benzaldehyde (250)		CO (170)		13
CTAB-ZnIn₂S₄[d]	Acetonitrile	benzyl alcohol	benzaldehyde (211); hydrobenzoin/benzoin (469)		CO (38)		14

(Table S3, Continued)

Catalyst	Solvent	Substrate	Oxidation product(s) (Yield(s) / μmol g^{-1} h^{-1})	Reduction product(s) (Yield(s) / μmol g^{-1} h^{-1})	Ref.
Cu/TiO$_2$	Acetonitrile		(1120)	CH$_3$OH (84)	15
Pd/TiO$_2$	gas phase	C$_2$H$_6$	C$_2$H$_4$ (230)	CO (120)	16
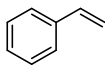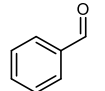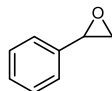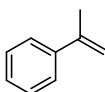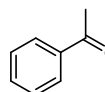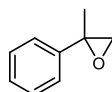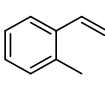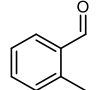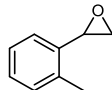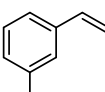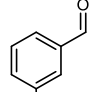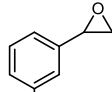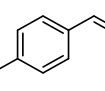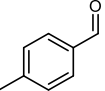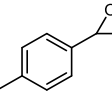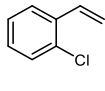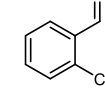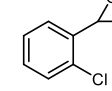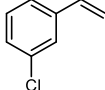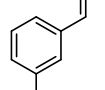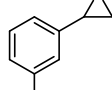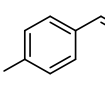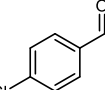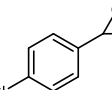
[a] g-CN/POM/[Re]: g-C$_3$N$_4$/H$_3$PW$_{12}$O$_{40}$/Re$_2$(bipyNNH$_2$bipy)(CO)$_6$Cl$_2$. [b] RGO: Reduced graphene oxide. [c] FAPbBr$_3$: Formamidinium lead bromide. [d] CTAB: Cetyl trimethyl ammonium bromide.

Table S4. Representative summary of photocatalytic styrene oxidation.

Oxidant	Solvent	Catalyst	Yield (μmol g^{-1} h^{-1})				Ref.
			BD	SO	CO	CH$_4$	
CO_2	Acetonitrile	BiOBr-NCN-S	684	139	802	8	This work
O_2	Acetonitrile	UiO-66-NH$_2$@MIL-101(Fe)	225	-	-	-	17
H_2O_2	Acetonitrile	PAN/Ag NPs/g-C$_3$N$_4$ NFs[a]	980	1838	-	-	18
O_2	n-Hexane	CsPbBr$_3$/Cs$_4$PbBr$_6$	1098	-	-	-	19
O_2	Tetrahydrofuran	Au/TiO$_2$ + RuCl$_3$·xH$_2$O	-	813	-	-	20
O_2	Acetonitrile + H$_2$O	BBT[b]	430	-	-	-	21
Air	N,N-dimethylformamide	BiC$_3$N$_3$S$_3$	274	1251	-	-	22

[a] PAN/Ag NPs/g-C$_3$N$_4$ NFs: Polyacrylonitrile/Ag nanoparticles/g-C$_3$N$_4$ nanofibers. [b] BBT: triethynylbenzene benzothiodiazole.

Table S5. The photocatalytic selective oxidation of different aromatic olefins coupled with CO_2 reduction over BiOBr-NCN-S catalyst [a].

Substrate	Products		Yields ($\mu mol\ g^{-1}$)			
A	B	C	B	C	CO	CH₄
			6636	1356	7658	81
			7080	1618	8374	83
			4020	1120	4982	38
			5454	1266	6484	61
			8088	1932	9564	112
			4308	858	4956	69
			5094	1048	5882	63
			6090	1232	6984	84

[a] Reaction condition: 0.1 mmol substrate, 5 mg BiOBr-NCN-S catalyst, in 5 mL acetonitrile, CO_2 atmosphere (0.1 MPa), 6 h, 25 °C, under Xe lamp irradiation.

References

1 G. Wang, Y. Wu, Z. Li, Z. Lou, Q. Chen, Y. Li, D. Wang, and J. Mao, *Angew. Chem. Int. Ed.*, 2023, **62**, e2022184.

2 L. Li, X. Dai, D. Chen, Y. Zeng, Y. Hu, and X. Lou, *Angew. Chem. Int. Ed.*, 2022, **61**, e2022058.

3 N. Huang, J. Shen, X. Zhang, P. Liao, J. Zhang, and X. Chen, *J. Am. Chem. Soc.*, 2022, **144**, 8676-8682.

4 J. Wang, T. Heil, B. Zhu, C. Tung, J. Yu, H. Chen, M. Antonietti, and S. Cao, *ACS Nano*, 2020, **14**, 8584-8593.

5 F. Wang, T. Hou, X. Zhao, W. Yao, R. Fang, K. Shen, and Y. Li, *Adv. Mater.*, 2021, **33**, 2102690.

6 X. Zhang, P. Wang, X. Lv, X. Niu, X. Lin, S. Zhong, D. Wang, H. Lin, J. Chen, and S. Bai, *ACS Catal.*, 2022, **12**, 2569-2580.

7 S. Gong, Y. Niu, X. Teng, X. Liu, M. Xu, C. Xu, T. Meyer, and Z. Chen, *Appl. Catal. B Environ.*, 2022, **310**, 121333.

8 J. Di, C. Chen, S. Yang, S. Chen, M. Duan, J. Xiong, C. Zhu, R. Long, W. Hao, Z. Chi, H. Chen, Y. Weng, J. Xia, L. Song, S. Li, H. Li, and Z. Liu, *Nat. Commun.*, 2019, **10**, 2840.

9 H. Yu, E. Haviv, and R. Neumann, *Angew. Chem. Int. Ed.*, 2020, **59**, 6219-6223.

10 L. Wang, X. Zhang, L. Yang, C. Wang, and H. Wang, *Catal. Sci. Technol.*, 2015, **5**, 4800-4805.

11 Y. Chen, M. Wang, Y. Ma, Y. Li, J. Cai, and Z. Li, *Catal. Sci. Technol.*, 2018, **8**, 2218-2223.

12 X. Li, D. Wei, L. Ye, and Z. Li, *Inorg. Chem. Commun.*, 2019, **104**, 171-177.

13 H. Huang, J. Zhao, Y. Du, C. Zhou, M. Zhang, Z. Wang, Y. Weng, J. Long, J. Hofkens, J. Steele, and M. Roeffaers, *ACS Nano*, 2020, **14**, 16689-16697.

14 L. Yuan, Y. Li, Z. Tang, J. Gong, and Y. Xu, *J. Catal.*, 2020, **390**, 244-250.

15 T. Yang, Q. Yu, and H. Wang, *Catal. Lett.*, 2018, **148**, 2382-2390.

16 R. Zhang, H. Wang, S. Tang, C. Liu, F. Dong, H. Yue, and B. Liang, *ACS Catal.*, 2018, **8**, 9280-9286.

17 L. Liu, L. Zhang, F. Wang, K. Qi, H. Zhang, X. Cui, and W. Zheng, *Nanoscale*, 2019, **11**, 7554-7559.

18 A. Shah, A. Sharma, V. Sharma, and N. Shimpi, *ACS Appl. Nano Mater.*, 2020, **3**, 1922-1933.

19 P. Qiu, Q. Wang, Y. Zhao, Y. Dai, Y. Dong, C. Chen, Q. Chen, and Y. Li, *Front. Chem.*, 2020, **8**, 130.

20 A. Graml, and B. König, *ChemPhotoChem*, 2021, **5**, 362-368.

21 C. Ayed, L. Silva, D. Wang and K. Zhang, *J. Mater. Chem. A*, 2018, **6**, 22145-22151.

22 Q. Wang, X. Deng, W. Chen, P. Chen, F. Liu, and S. Yin, *Fuel*, 2021, **302**, 121127.